Molecular Biology of the Cell
Vol. 9, 2439–2461, September 1998

A Novel Fluorescence-based Genetic Strategy Identifies Mutants of *Saccharomyces cerevisiae* Defective for Nuclear Pore Complex Assembly

Mirella Bucci and Susan R. Wente*

Department of Cell Biology and Physiology, Washington University School of Medicine, St. Louis, Missouri 63110

Submitted January 14, 1998; Accepted June 9, 1998
Monitoring Editor: Pamela A. Silver

Nuclear pore complexes (NPCs) are large proteinaceous portals for exchanging macromolecules between the nucleus and the cytoplasm. Revealing how this transport apparatus is assembled will be critical for understanding the nuclear transport mechanism. To address this issue and to identify factors that regulate NPC formation and dynamics, a novel fluorescence-based strategy was used. This approach is based on the functional tagging of NPC proteins with the green fluorescent protein (GFP), and the hypothesis that NPC assembly mutants will have distinct GFP-NPC signals as compared with wild-type (wt) cells. By fluorescence-activated cell sorting for cells with low GFP signal from a population of mutagenized cells expressing GFP-Nup49p, three complementation groups were identified: two correspond to mutant *nup120* and *gle2* alleles that result in clusters of NPCs. Interestingly, a third group was a novel temperature-sensitive allele of *nup57*. The lowered GFP-Nup49p incorporation in the *nup57-E17* cells resulted in a decreased fluorescence level, which was due in part to a sharply diminished interaction between the carboxy-terminal truncated nup57p^{E17} and wt Nup49p. Interestingly, the *nup57-E17* mutant also affected the incorporation of a specific subset of other nucleoporins into the NPC. Decreased levels of NPC-associated Nsp1p and Nup116p were observed. In contrast, the localizations of Nic96p, Nup82p, Nup159p, Nup145p, and Pom152p were not markedly diminished. Coincidentally, nuclear import capacity was inhibited. Taken together, the identification of such mutants with specific perturbations of NPC structure validates this fluorescence-based strategy as a powerful approach for providing insight into the mechanism of NPC biogenesis.

INTRODUCTION

The exchange of macromolecules between the nuclear and cytoplasmic compartments is mediated by nuclear pore complexes (NPCs)[1] embedded in ~90-nm-diameter pores within the double lipid bilayer of the nuclear envelope (NE). Each NPC is a cylindrical structure with a superficial octagonal symmetry characterized by distinct substructures referred to as spokes, rings, a central plug, cytoplasmic fibrils, and a nuclear basket (Ris, 1991; Hinshaw *et al.*, 1992; Akey and Radermacher, 1993; Akey, 1995; Goldberg and Allen, 1995; Pante and Aebi, 1996). NPCs are believed to be functionally similar in all eukaryotic organisms. Based on the polypeptide complexity of purified yeast complexes (Rout and Blobel, 1993), an NPC may be comprised of at least 50 distinct proteins [called nucleoporins (NUPs)]. To date, at least 25 nucleoporins have been identified in the yeast *Saccharomyces cerevisiae* with a comparatively smaller fraction identified in higher eukaryotes (reviewed by Corbett and Silver, 1997; Doye and Hurt 1997). While this knowledge of the physical composition of the NPC continues to grow, much less is known about the molecular basis of how nucleoporins are brought together and how

* Corresponding author.
[1] Abbreviations used: GFP, green fluorescent protein; NPC, nuclear pore complex; NE, nuclear envelope; wt, wild-type.

this is coordinated with insertion of these macromolecular structures into the NE pore. A precise understanding of NPC transport function will require integrating the location and assembly interactions of nucleoporins into the context of NPC architecture.

Vertebrate cell-free systems have provided excellent models for studying NPC biogenesis (Lohka and Masui, 1983; Miake-Lye and Kirschner, 1985; Burke and Gerace, 1986; Suprynowicz and Gerace, 1986; Newport 1987). NPC assembly and disassembly can be reconstituted in vitro from vertebrate cell extracts, and a general framework for the stages of NPC assembly has been revealed. NPC assembly requires the prior formation of a double nuclear membrane (Macaulay and Forbes, 1996) and is inhibited by the addition of GTPγS, BAPTA (a chelator of Ca^{++} and Zn^{++}), or wheat germ agglutinin (Newmeyer and Forbes, 1990; Pfaller *et al.*, 1991; Newport and Dunphy, 1992; Boman *et al.*, 1992a,b; Vigers and Lohka, 1992; Sullivan *et al.*, 1993; Macaulay and Forbes, 1996; Goldberg *et al.*, 1997). Depletion of either vesicular or soluble components from the in vitro extracts can also prevent NPC formation (Sheehan *et al.*, 1988; Dabauvalle *et al.*, 1990; Finlay and Forbes, 1990; Finlay *et al.*, 1991; Vigers and Lohka, 1991), yet purification of any assembly factors has not been accomplished.

Based on the models for NPC ultrastructure (Macaulay and Forbes, 1996; Goldberg *et al.*, 1997), interactions between integral membrane proteins are likely required for formation of the pore. Association of individual nucleoporins and integral membrane proteins is presumed essential for anchoring a NPC in the NE pore. Candidates for mediators of NPC assembly and dynamics have been revealed by either molecular analysis of NPC proteins or characterization of yeast mutant phenotypes. Yeast Pom152p and vertebrate Pom121p and gp210 are integral membrane proteins that localize to the pore membrane and may mediate the anchorage of NPCs in the NE (Gerace *et al.*, 1982; Wozniak *et al.*, 1989; Greber *et al.*, 1990; Hallberg *et al.*, 1993; Wozniak *et al.*, 1994). Peripheral membrane proteins with potential roles in NPC biogenesis include those in which NPC and/or NE structure is perturbed in the respective mutant strains (reviewed in Corbett and Silver, 1997; Doye and Hurt, 1997; Wente *et al.*, 1997). In some cases, these mutant phenotypes may reflect direct effects on NPC biogenesis such that assembly is inhibited and/or accumulation of assembly intermediates results. For example, depletion of the essential yeast nucleoporin Nsp1p or *NIC96* mutant alleles results in a reduction in NPC density (Mutvei *et al.*, 1992; Zabel *et al.*, 1996). Recently, mammalian and *Xenopus* homologues of yeast Nic96p have been identified, and immunodepletion of the *Xenopus* protein from nuclear/NPC assembly extracts further suggests that it plays a role in the biogenesis of wild-type (wt) NPCs (Grandi *et al.*, 1997). Interestingly, clusters of NPCs in aggregated patches of NE are present in yeast cells expressing mutant alleles of *nup145, nup133, nup120, nup159, nup84, nup85,* and *gle2* (Doye *et al.*, 1994; Wente and Blobel, 1994; Aitchison *et al.*, 1995; Gorsch *et al.*, 1995; Heath *et al.*, 1995; Li *et al.*, 1995; Pemberton *et al.*, 1995; Goldstein *et al.*, 1996; Murphy *et al.*, 1996; Siniossoglou *et al.*, 1996). We recently determined that for one yeast mutant (*gle2*) (Murphy *et al.*, 1996), NPC clustering results from the migration of pre-existing NPCs into aggregates rather than from the assembly of new NPCs into a fixed site on the NE (Bucci and Wente, 1997). All of the known yeast clustering mutants are defective in a specific NPC-associated factor. However, a *Drosophila melanogaster* mutant for a component of the nuclear lamina has recently been shown to result in NPC clusters (Lenz-Bohme *et al.*, 1997). In addition, a yeast *act2* mutant allele was described that causes abnormal NPC morphology and nucleoporin stoichiometry (Yan *et al.*, 1997). These results suggest that both NPC and non-NPC components can contribute to proper NPC assembly and/or maintenance of proper NPC ultrastructure.

To date, direct genetic screens for global mediators of NPC biogenesis have not been conducted. All of the reported NPC structural perturbations in yeast cells have been found as a matter of course during the characterization of the particular genes. We have developed a new strategy specifically directed at isolating NPC biogenesis mutants using an unbiased fluorescence strategy. This approach is based on the functional tagging of nucleoporins with the green fluorescent protein (GFP) and the hypothesis that NPC assembly mutants expressing the GFP-nucleoporin will have distinct fluorescence signals as compared with wt cells. We selected for such mutants by fluorescence-activated cell sorting (FACS) from a mutagenized population of *S. cerevisiae* cells expressing GFP-Nup49p and identified novel *nup120*, *gle2*, and *nup57* alleles. The temperature-sensitive *nup57-E17* cells have a lowered GFP fluorescence due to decreased NPC incorporation of GFP-Nup49p. The consequences of this perturbation were further characterized and revealed an in vivo network of interactions that mediate NPC structural integrity. Overall, the results exemplify our ability to identify in vivo mediators of NPC structure and assembly.

MATERIALS AND METHODS

Plasmids

All plasmids were made by standard methods (Sambrook *et al.*, 1989), and DH5α was used as the bacterial host. The plasmids were generated as follows:

pSW242 (*NUP49/LEU2/2*μ): insertion of a 2,415-base pair (bp) *Bam*HI/*Sal*I fragment containing *NUP49* locus from pSW40 (Wente *et al.*, 1992) into pRS425 (Christianson *et al.*, 1992).

pSW490 (*NUP57/TRP1/CEN*): insertion of a *Sal*I/*Xho*I digested ~2,960-bp *NUP57* fragment made by PCR using oligonucleotide primers 57–1 (GATAACTTTGATGTCGACAGATTCC) and 57–2 (ACGAAAGTTATCCTCTCGAGGACAC), into pRS314 (Sikorski and Hieter, 1989).

pSW626 (*GFP-S65T* in pBS-SK): insertion of the 756-bp *Eco*RI fragment from GFP-S65T in pRSET$_B$ (Heim and Tsien, 1996) into *Eco*RI-digested pBS-SK.

pSW634 (*GFP-S65T/kan*^{r} in pBS-SK): *Not*I digestion of pSW626 and insertion of the 1,619-bp *Not*I fragment from pUG6 (Guldener *et al.*, 1996).

pSW636 (*GFP-NUP49/LEU2/CEN*): insertion of the 1,763-bp *Xba*I fragment from pSW442 (Bucci and Wente, 1997) into *Xba*I-digested pSW62 (Wente *et al.*, 1992).

pSW639 (*GFP-F64L,S65T/kan*^{r} in pBS-SK): insertion of the 756-bp *Eco*RI fragment from GFP-F64L,S65T in pRSET$_B$ (Heim and Tsien, 1996) into *Eco*RI-digested pSW634.

pSW806 (*NUP57/LEU2/CEN*): insertion of the ~2,950-bp *Xho*I/*Not*I fragment from pSW490 into pRS315 (Sikorski and Hieter, 1989).

pSW860 (*NUP57* in pQE-32) and pSW862 (*nup57-E17* in pQE-32): insertion of *Kpn*I fragments generated by PCR using yeast SWY809 and SWY1586, respectively, as genomic template with oligonucleotides QEA (CAAGGTACCACATGTTTGGTTTCA) and QEB (CTCGGTACCCTCCTTGTTGGCTTTGTG) to amplify the entire open reading frames and ~360 bp of 3′-untranslated region generating a fusion to the His$_6$ tag, in pQE32 (QIAGEN, Chatsworth, CA).

pSW921 (*NUP49-C* in pACTII): insertion of a ~848-bp *Bam*HI fragment generated by PCR with oligonucleotide primers 49–2 (AGCGGATCCTGCAGCAACAACCACAA) and 49.B2 (AAAGGATCCTCGGCCTCTAAGACGCC) (encoding for the Nup49p C-terminus (last 253 amino acids of the protein), into pACTII.

pSW924 (*NUP57* in pCH432) and pSW925 (*nup57-E17* in pCH432): insertion into pCH432 (Hardy, 1996) of *Bgl*II fragments generated by PCR with oligonucleotide primers 2HB1 (GACAGATCTATCACATGTTTGGTTT) and 2HB2 (AAGAGATCTGGTGTCTCCTTGTTGG) and pSW860 or pSW682 as templates, respectively, for in-frame fusion to the DNA-binding domain of LexA.

pSW950 (*GFP-NIC96/HIS3*): insertion of three fragments into the *HIS3* integrating vector pRS303 (Christianson *et al.*, 1992). The first fragment was prepared by *Xho*I/*Sac*I digestion of a PCR product including 528 bp of 5′ *NIC96* promoter sequence and the initiation methionine. The second fragment was prepared by *Xho*I digestion of a PCR product made using oligonucleotide primers GFP-C (GTACTGCAGGATCCTCGAGATGAGTAAAGGAGAAGAA) and GFP-E (TTTCTGCAGGATCCTCGAGGGTTTGTATAGTTCATCCAT) and contains the full open reading frame of GFP-S65T. The final fragment was generated by *Xho*I/*Bam*HI digestion of a PCR product created using oligonucleotide primers NIC96–6 (TGTGGATCCATTTAAAAGCTGTTCGATAGAC) and NIC96–7 (GGACTCGAGGGCTGCGCGCGGAAATAAGCTGCAT). This product contains two alanine residues followed by 379 bp of the *NIC96* coding sequence just downstream of the initiation methionine.

pSW956 (*GFP-NSP1/HIS3*): insertion of three fragments into the *HIS3* integrating vector pRS303. The first fragment was prepared by *Xho*I/*Sac*I digestion of a PCR product made using oligonucleotide primers NSP1–3 (TCCGAGCTCCACAGGCTCCAATACTTCTAGAA) and NSP1–7 (CGACTCGAGCGCAGCCGTTTTGTTTTGTTGAGG) and includes ~ 503 bp of *NSP1* promoter and intron sequence as well as the first 11 codons of *NSP1*, followed by two alanine residues. The second fragment containing GFP-S65T was prepared using oligonucleotide primers GFP-C and GFP-E as described above. The last fragment was prepared by *Xho*I/*Stu*I digestion of a PCR product made using oligonucleotide primers NSP1-C (GTCGAGTCGACTGGTGCGTATTTACTGTC) and NSP1–8 (GGACTCGAGTGCTGCGACGGGGAAGTCAACCGC) and encodes for two alanine residues and amino acids 606–823 of Nsp1p.

Other plasmids used in this study include: pSW406 (*GLE2/LEU2/CEN*) (Murphy *et al.*, 1996); pCH4 (*NUP120/LEU2/CEN*) (Heath *et al.*, 1995); pNLS-E1 (*NLS-LacZ/URA3/2μ*) (Underwood and Fried, 1990); pCH428 (*LexA-ORC2/TRP1/2μ*) (Hardy, 1996); pSE1111 (*GAL4*$_{AD}$-*SNF4/LEU2/2μ*) (Yang *et al.*, 1992).

Yeast Strains

General yeast manipulations were conducted by standard methods (Sherman *et al.*, 1986) with transformations by the lithium acetate method (Ito *et al.*, 1983). Yeast strains were grown in either rich YPD (yeast extract, peptone, 2% dextrose) or synthetic complete (SC) medium supplemented with 2% sugar (SD, dextrose) when GFP fluorescence was monitored. Mutant strains with temperature-conditional defects were maintained at 23°C unless otherwise noted. The *S. cerevisiae* strains used in this study are described in Table 1 and as follows. To achieve minimal autofluorescence, all yeast strains used for GFP fluorescence analysis were adenine prototrophs.

The *nup133Δ::HIS3* strains was made by the gene deletion method of Baudin *et al.* (1993) using oligonucleotides 133D1 (TATGAAGAGGAAAGCCAGGCCTCTCTAATGGACATTTCCATGGAGGGCCTCCTCTAGTACACTC) and 133D2 (GTATTCTACAGTGTTGGTTTCATAGTTGATGGTATAGTTTTTTTCGCGCGCCTCGTTCAGAATG), which anneal at their 3′-ends to the *HIS3* locus in pBM2815 (generous gift of Linda Riles, Washington University, St. Louis, MO). PCR generated a 1100-bp fragment flanked on the 5′-end with sequences complementary to *NUP133* bp 1042–1086, including the initiation methionine and on the 3′-end with sequences complimentary to *NUP133* bp 4378–4422 just before the TAA stop codon. W303 **a**/α was transformed with the PCR product to create SWY422. Genomic colony PCR confirmed correct chromosomal integration.

C-terminal tagging of Nup82p with GFP was achieved by the gene integration method of Baudin *et al.* (1993). wt SWY595 cells were transformed with a PCR product generated with oligonucleotides NUP82-G (TTGTTACAAGTTTCTCAGGAATTTACTACTAAAACTCAAGCTGCGATGAGTAAAGGAGAAGAA) and NUP82-K (CCGAGAGACACGATCTGTAGCGGTGATATGAACGTATTCCTCACCCAGCTGAAGCTTCGTACGC) using pSW639 as template. This template contained the GFP-F64L, S65T coding sequence and the *kan*^{r} cassette. Sequences flanking the PCR product are complementary to nucleotides of the *NUP82* locus and placed two alanine residues, and GFP-F64L, S65T, in frame with the *NUP82* open reading frame. G418-resistant transformants were selected, and integration at the *NUP82* locus was confirmed by PCR.

N-terminal tagging of Nic96p with GFP was completed by chromosomal integration of AflII-digested pSW950. This creates an in-frame fusion of GFP, two alanine residues and the chromosomal copy of NIC96 separated from a truncated NIC96 gene by sequences corresponding to the integrating vector pRS303. Replacement of the N terminus of Nsp1p with GFP was completed by chromosomal integration of SpeI-digested pSW956. This created an in-frame fusion of the first 11 codons of NSP1 with two alanine residues and GFP followed by codons encoding two alanine residues and Nsp1p residues 607 to the end.

Flow Cytometry and FACS Screening

Logarithmically grown yeast cells expressing GFP-Nup49p were analyzed by flow cytometry using a FACScan flow cytometer (Becton Dickinson, Franklin Lakes, NJ). For enrichment of mutants, ~4×10^7 SWY809 and SWY811 cells were mutagenized in 3% EMS and 100 mM potassium phosphate, pH 7.0, to ~60% viability. After 24 h of incubation in liquid culture at 23°C, the cells were briefly sonicated and then selected by FACS with an Epics 753 flow cytometer (Coulter Electronics, Hialeah, FL). The cells were excited at 488 nm by an argon ion laser (Coherent, Santa Clara, CA), and the emitted light was passed through a 530/30 bandpass filter. A forward scatter threshold was used to select events for acquisition, and forward and side scatter gates were used to restrict analysis to single events. Approximately 1% of the total cells were sorted from those cells having the lowest GFP fluorescence, and ~10% of the

Table 1. Yeast strains used in this study

Strain	Genotype	Derivation
CHY104	*Mat***a** *ura3-52 his3Δ200 leu2Δ1 NUP120::HIS3*	Heath *et al*., 1995
L40	*Mat***a** *his3Δ200 trp1-901 leu2-3,112 ade2 LYS2::(LexA$_{op}$)$_4$-HIS3 URA3::(LexA$_{op}$)$_8$-LacZ*	S. Hollenberg
*nic*96-1	*Mat***a** *ade2 trp1 leu2 ura3 HIS3::nic96 (pUN100-LEU2-nic96^{ts} [P332L;L260P])*	Zabel *et al*., 1996
SWY422	*Mat***a**/*Matα ade2-1/ade2-1 ura3-1/ura3-1 his3-11,15/his3-11/15 trp1-1/trp1-1 leu2-3,112/leu2-3,112 can1-100/can1-100 nup133Δ::HIS3/nup133*	Chromosomal integration of HIS3 at *NUP133* locus
SWY423	*Matα ade2-1 ura3-1 his3-11,15 trp1-1 leu2-3,112 can1-100 nup133Δ::HIS3*	Segregant of SWY422
SWY458	*Mat***a** *ura3-1 his3-11,15 trp1-1 leu2-3,112 can1-100 ade2-1:ADE2-URA3*	Bucci and Wente, 1997
SWY459	*Matα ura3-1 his3-11,15 trp1-1 leu2-3,112 can1-100 ade2-1:ADE2-URA3*	Bucci and Wente, 1997
SWY518	*Mat***a** *ura3-1 his3-11,15 trp1-1 leu2-3,112 can1-100 ade2-1:ADE2*	Bucci and Wente, 1997
SWY519	*Matα ura3-1 his3-11,15 trp1-1 leu2-3,112 can1-100 ade2-1:ADE2*	Bucci and Wente, 1997
SWY595	*Mat***a**/*MATα ura3-1/ura3-1 his3-11,15/his3-11,15 trp1-1/trp1-1 leu2-3,112/leu2-3,112 can1-100/can1-100 ade2-1:ADE2/ade2-1:ADE2*	Bucci and Wente, 1997
SWY729	*Matα ade2-1:ADE2-URA3 ura3-1 his3-11,15 trp1-1 leu2-3,112 can1-100 nup133Δ::HIS3*	Transformation of SWY423 with the integrating vector pSW286 (Bucci and Wente, 1997)
SWY734	*Mat***a** *ade2-1 ura3-1 his3-11,15 trp1-1 leu2-3,112 can1-100 nup49-1::URA3 nup49ΔGLFG::GFP-S65T-TRP1*	Bucci and Wente, 1997
SWY737	*Matα ade2-1 ura3-1 his3-11,15 trp1-1 leu2-3,112 can1-100 nup49-1::URA3*	Bucci and Wente, 1997
SWY760	*Matα ura3-1 his3-11,15 trp1-1 leu2-3,112 can1-100 ade2-1:ADE2-URA3 pSW242 (LEU2)*	SWY459 transformed with pSW242
SWY809	*Mat***a** *ura3-1 his3-11,15 trp1-1 leu2-3,112 can1-100 ade2-1:ADE2 nup49-1::URA3 nup49ΔGLFG::GFP-S65T-TRP1*	Bucci and Wente, 1997
SWY811	*Matα ura3-1 his3-11,15 trp1-1 leu2-3,112 can1-100 ade2-1:ADE2 nup49-1::URA3 nup49ΔGLFG::GFP-S65T-TRP1*	Segregant of diploid created by crossing SWY737 with SWY518
SWY828	*Mat***a** *ura3-1 his3-11,15 trp1-1 leu2-3,112 can1-100 ade2-1:ADE2-URA3 nup49-1::URA3 nup49ΔGLFG::GFP-S65T-TRP1 nup133Δ::HIS3*	Segregant of diploid created by crossing SWY729 with SWY734
SWY894	*Mat***a** *ura3-1 his3-11,15 trp1-1 leu2-3,112 can1-100 ade2-1:ADE2 nup49-1::URA3 nup49ΔGLFG::GFP-S65T-TRP1 pRS315 (LEU2)*	SWY809 transformed with pRS315
SWY1186	*Mat***a** *ade2-1 ura3-1 his3-11,15 trp1-1 leu2-3,112 lys2 gle1-4*	Murphy and Wente, 1996
SWY1226	*Matα ade2-1 ura3-1 his3-11,15 leu2-3,112 trp1-1 can1-100 GLE2Δ::HIS3*	Murphy *et al*., 1996
SWY1427	*Mat***a**/*Matα ura3-1/ura3-1 his3-11,15/his3-11,15 trp1-1/trp1-1 leu2-3,112/leu2-3,112 can1-100/can1-100 ade2-1:ADE2/ade2-1:ADE2 NUP82-GFP-F64L, S65T-kan^R/NUP82*	SWY595 transformed with the PCR product created with oligos NUP82G and NUP82K using pSW639 as template
SWY1441	*Mat***a** *ura3-1 his3-11,15 trp1-1 leu2-3,112 can1-100 ade2-1:ADE2 NUP82-GFP-F64L,S65T-kan^R*	Segregant of SWY1427
SWY1511	*Mat***a** *ura3-1 his3-11,15 trp1-1 leu2-3,112 can1-100 ade2-1:ADE2 NUP82-GFP-F64L,S65T-kan^R pRS425 (LEU2)*	SWY1441 transformed with pRS425
SWY1586	*Matα ura3-1 his3-11,15 trp1-1 leu2-3,112 can1-100 ade2-1:ADE2 nup57-E17 nup49-1::URA3 nup49ΔGLFG::GFP-S65T-TRP1*	Segregant of a backcross between SWY811 and the *nup57-E17* clone obtained from mutagenesis of SWY809
SWY1587	*Matα ura3-1 his3-11,15 trp1-1 leu2-3,112 can1-100 ade2-1:ADE2 nup57-E17*	Segregant of a backcross between SWY760 and the *nup57-E17* clone obtained from mutagenesis of SWY809
SWY1601	*Mat***a** *ura3-1 his3-11,15 trp1-1 leu2-3,112 can1-100 ade2-1:ADE2-URA3 pRS315 (LEU2)*	SWY458 transformed with pRS315
SWY1667	*Mat***a** ura3-1 his3-11,15 trp1-1 leu2-3,112 can1-100 ade2-1:ADE2-URA3 nup49-1::URA3 nup49ΔGLFG::GFP-S65T-TRP1 nup133Δ::HIS3 pRS315 (LEU2)	SWY828 transformed with pRS315
SWY1693	*Mat***a**/*Matα ura3-1/ura3-1 his3-11,15/his3-11,15 trp1-1/trp1-1 leu2-3,112/leu2-3,112 can1-100/can1-100 ade2-1:ADE2/ade2-1:ADE2 GFP-S65T-NIC96-HIS3/NIC96*	SWY595 transformed with *Afl*II-digested pSW950
SWY1695	*Mat***a** *ura3-1 his3-11,15 trp1-1 leu2-3,112 can1-100 ade2-1:ADE2 GFP-S65T-NIC96-HIS3*	Segregant of SWY1693
SWY1705	*Mat***a** *ura3-1 his3-11,15 trp1-1 leu2-3,112 can1-100 ade2-1:ADE2 nup49-1::URA3 nup49ΔGLFG::GFP-S65T-TRP1 gle2-C18 pRS315 (LEU2)*	Mutagenesis of SWY809 and transformation with pRS315
SWY1706	*Mat***a** *ura3-1 his3-11,15 trp1-1 leu2-3,112 can1-100 ade2-1:ADE2 nup49-1::URA3 nup49ΔGLFG::GFP-S65T-TRP1 gle2-C18 pSW406 (LEU2)*	Mutagenesis of SWY809 and transformation with pSW406
SWY1707	*Matα ura3-1 his3-11,15 trp1-1 leu2-3,112 can1-100 ade2-1:ADE2 nup49-1::URA3 nup49ΔGLFG::GFP-S65T-D66-TRP1 pRS315 (LEU2)*	Mutagenesis of SWY811, one backcross to SWY809, and transformation with pRS315
SWY1708	*Matα ura3-1 his3-11,15 trp1-1 leu2-3,112 can1-100 ade2-1:ADE2 nup57-E17 nup49-1::URA3 nup49ΔGLFG::GFP-S65T-TRP1 pRS315 (LEU2)*	SWY1586 transformed with pRS315
SWY1709	*Matα ura3-1 his3-11,15 trp1-1 leu2-3,112 can1-100 ade2-1:ADE2 nup57-E17 nup49-1::URA3 nup49ΔGLFG::GFP-S65T-TRP1 pSW806 (LEU2)*	SWY1586 transformed with pSW806
SWY1710	*Matα ura3-1 his3-11,15 trp1-1 leu2-3,112 can1-100 ade2-1:ADE2 nup49-1::URA3 nup49ΔGLFG::GFP-S65T-TRP1 nup120-C36 pRS315 (LEU2)*	Mutagenesis of SWY811 and transformation with pRS315

Table 1. *Continued*

Strain	Genotype	Derivation
SWY1711	*Matα ura3-1 his3-11,15 trp1-1 leu2-3,112 can1-100 ade2-1:ADE2 nup49-1::URA3 nup49ΔGLFG::GFP-S65T-TRP1 nup120-C36 pCH4 (LEU2)*	Mutagenesis of SWY811 and transformation with pCH4
SWY1717	*Mat**a**/Matα ura3-1/ura3-1 his3-11,15/his3-11,15 trp1-1/trp1-1 leu2-3,112/leu2-3,112 can1-100/can1-100 ade2-1:ADE2/ade2-1:ADE2 nsp1ΔN::GFP-S65T-HIS3/NSP1*	SWY595 transformed with *Spe*I-digested pSW956
SWY1722	*Mat**a** ura3-1 his3-11,15 trp1-1 leu2-3,112 can1-100 ade2-1:ADE2 nup57-E17 GFP-S65T-NIC96-HIS3*	Segregant of a diploid created by crossing SWY1695 and SWY1586
SWY1728	*Matα ura3-1 his3-11,15 trp1-1 leu2-3,112 can1-100 ade2-1:ADE2 nsp1ΔN:GFP-S65T-HIS3*	Segregant of SWY1717
SWY1729	*Mat**a** ura3-1 his3-11,15 trp1-1 leu2-3,112 can1-100 ade2-1:ADE2 nsp1ΔN::GFP-S65T-HIS3*	Segregant of SWY1717
SWY1736	*Matα ura3-1 his3-11,15 trp1-1 leu2-3,112 can1-100 ade2-1:ADE2 nup57-E17 nsp1ΔN::GFP-S65T-HIS3*	Segregant of a diploid created by crossing SWY1729 and SWY1586
SWY1744	*Matx ura3-1 his3-11,15 trp1-1 leu2-3,112 can1-100 ade2-1:ADE2 nup57-E17 NUP82-GFP-F64L,S65T-kan^R pRS425 (LEU2)*	Segregant of a diploid created by crossing SWY1511 and SWY1586
SWY1824	*Mat**a** ura3-1 his3-11,15 trp1-1 leu2-3,112 can1-100 ade2-1:ADE2-URA3 nup133Δ::HIS3 GFP-S65T-NIC96-HIS3*	Segregant of a diploid created by crossing SWY729 and SWY1695
SWY1860	*Mat**a** ura3-1 his3-11,15 trp1-1 leu2-3,112 can1-100 ade2-1:ADE2 nup49-1::URA3 nup49ΔGLFG::GFP-S65T-TRP1 HIS3::nic96 (pUN100-LEU2-nic96^{ts} [P332L;L26P])*	Segregant of a diploid created by crossing SWY811 and *nic96-1*

sorted cells formed colonies on YPD plates at 23°C. Approximately 1000 cells from each mating type were screened by direct fluorescence microscopy at 23°C for NPC defects including clustering and low NPC-associated GFP-Nup49p. Eight mutants (2 from the *MATα* strain, 6 from the *MAT**a*** strain) found in the visual screen were tested for sensitivity to various temperatures and for complementation by a plasmid encoding GFP-Nup49p and a panel of plasmids encoding NPC-associated components.

Microscopic Characterization of Mutants

GFP fluorescence was visualized directly after fixation of cells for 10 min in 3.7% formaldehyde and 10% methanol. Indirect immunofluorescence staining of yeast cells was performed essentially as described (Wente *et al.*, 1992). Cells were fixed for 10 min in 3.7% formaldehyde and 10% methanol before or after shifts to 37°C. Primary antibodies used were graciously provided from colleagues and used at the following dilutions for 16-h incubations at 4°C: monoclonal anti-Pom152p (mAb 118C3 tissue culture supernatant, undiluted) (Strambio-de-Castillia *et al.*, 1995), monoclonal anti-Nup159p (mAb 165C10, tissue culture supernatant, undiluted) (Kraemer *et al.*, 1995), affinity-purified rabbit polyclonal WU956 raised against the GLFG region of Nup116p (anti-GLFG, 1:200) (provided by J. Watkins, Washington University, St. Louis MO), affinity-purified rabbit polyclonal WU598 raised against the C-terminal region of Nup145p (1:20) (Emtage *et al.*, 1997), affinity-purified rabbit polyclonal WU600 raised against the C-terminal region of Nup116p (1:10) (Iovine *et al.*, 1995), and rabbit polyclonal WU1079 raised against the C-terminal region of Nup57p (1:200) (provided by J. Watkins, Washington University, St. Louis, MO). FITC-conjugated donkey anti-rabbit and goat anti-mouse antibodies (Cappel, Durham, NC) were used to detect the primary antibodies (1:200 dilutions). Photographs were taken using Kodak T-MAX 400 film on an Olympus microscope through a UPlanFL 100× 1.3 NA objective.

Electron microscopy was conducted essentially as described (Wente and Blobel, 1993). Briefly, cells were grown to early logarithmic phase in YPD at 23°C before shifting to 37°C for 4 h. Cells were immediately fixed with 2% glutaraldehyde, 2% formaldehyde (incubation on ice overnight). After cell wall digestion and osmium postfixation, the samples were embedded in EPON. Thin sections collected on nickel grids coated with formvar, stabilized with carbon, were contrasted with uranyl acetate and Reynold's lead. Specimens were visualized with a Zeiss-902 electron microscope (Carl Zeiss, Thornwood, NY), and photographs were recorded with Kodak electron microscopy film.

Characterization of nup57p^{E17}

The *nup57-E17* mutation was sequenced by the dideoxy chain termination method (Sanger *et al.*, 1977) using the Sequenase kit (Version 2, United States Biochemical, Cleveland, OH) and oligonucleotide primers 57–4 (AGCAGATCTCAGTACCGTTGCAACAAACGCAAGC) and 57–7 (CAATTGCAGCATCTTTC), annealing within the *nup57-E17* gene of pSW862. To compare expression levels of Nup57p and nup57p^{E17}, total yeast cell extracts and immunoblotting were conducted as described (Iovine *et al.*, 1995) after shifts for various times at 37°C in YPD. The affinity-purified rabbit polyclonal anti-GLFG antibodies (raised against the GLFG region of Nup116p, WU956) were used at a dilution of 1:1000. The GFP-Nup49p was recognized by a commercial polyclonal antibody recognizing GFP (1:500, CLONTECH, Palo Alto, CA). Bands were visualized by developing with nitro blue tetrazolium and 5-bromo-4-chloro-3-indolyl-1-phosphate (Promega, Madison, WI). For biochemical analysis of soluble versus insoluble/nuclear pools of given nucleoporins in wt and *nup57-E17* cells, yeast spheroplasts were osmotically lysed, fractionated by low-speed centrifugation, and extracted with 1 M NaCl as described by Bogerd *et al.* (1994). Protein samples were separated by electrophoresis in SDS-polyacrylamide gels and transferred to nitrocellulose membranes. Immunoblotting was conducted with the polyclonal anti-GFP antibody (CLONTECH) for GFP-Nup49p and GFP-Nsp1p, the polyclonal anti-GLFG antibody for Nup116p (WU956), guinea pig polyclonal antibody recognizing Nup159p (1:10,000) (Gorsch *et al.*, 1995) with a rabbit anti-guinea pig secondary (1:1000, Cappel), an affinity-purified rabbit polyclonal antibody recognizing the C-terminal region of Nup145p (Nup145-Cp) (1:100, WU599, Emtage *et al.* 1997), and an affinity-purified rabbit polyclonal antibody recognizing the C-terminal region of the integral membrane protein Snl1p (1:1000, WU975, Ho *et al.*, 1998). Bands were visualized by the ECL system (Amersham, Arlington Heights, IL) according to manufacturer's directions, and the autoradiographs were digitized and quantified using NIH Image (developed at the United States National Institutes of Health and available from the Internet by anonymous FTP from zippy.nimh.gov).

For the two-hybrid interaction analysis, yeast strain L40 was cotransformed with plasmids encoding Gal4p transcriptional activation domain fusions ($GAL4_{AD}$) and LexAp DNA-binding domain fusions ($LexA_{BD}$). Quantitative analysis of the β-galactosidase activity was determined as described previously (Guarente, 1983).

Nuclear Transport Assays

Analysis of nuclear import and export was completed essentially as described (Iovine *et al.*, 1995). Briefly, nuclear import capacity was assessed by monitoring the localization of a *GAL10*-induced nuclear localization sequence (NLS) β-galactosidase fusion protein (pNLS-E1) (Underwood and Fried, 1990). Yeast strains transformed with pNLS-E1 were grown in SC media lacking uracil with 2% raffinose for 2.5 h at 37°C. The cells were then shifted into SC media lacking uracil with 2% galactose for an additional 3.5 h at 37°C. The cells were processed for indirect immunofluorescence microscopy as described above with a primary mouse monoclonal anti-β-galactosidase antibody (ascites at 1:100, Sigma, St. Louis, MO), and a secondary rhodamine-conjugated donkey anti-mouse (Cappel). Nuclear export capacity was monitored in strains grown in YPD by the localization of poly(A)+ RNA as previously described (Wente and Blobel, 1993). In situ hybridization was conducted with an oligonucleotide poly$(dT)_{30}$ probe end labeled with digoxigenin-11-dUTP (Boehringer Mannheim, Mannheim, Germany) by terminal transferase (GIBCO BRL, Gaithersburg, MD). Detection of the probe was achieved using anti-digoxigenin-rhodamine FAb fragments (Boehringer Mannheim).

RESULTS

Rationale for a Fluorescence-based Genetic Strategy to Isolate NPC Mutants

To understand the molecular basis of NPC assembly and to identify mediators of NPC biogenesis, we previously developed assays to monitor NPCs in live cells of the yeast *S. cerevisiae* (Bucci and Wente, 1997). The nucleoporin Nup49p was functionally tagged with the GFP from *Aequora victoria*, expressed in yeast cells, and GFP-tagged NPC movement and assembly rates were monitored in live cells. We also expressed the GFP-Nup49p in a *gle2* temperature-dependent NPC clustering mutant and observed the dynamics of mutant GFP-tagged NPCs. During this analysis, we speculated that NPC assembly mutants may have distinct GFP fluorescence properties compared with wt cells. We predicted that if a wt strain expressing a GFP-tagged nucleoporin was mutagenized, at least three different classes of mutants might be distinguishable by their fluorescence properties. Mutants that result in NPC clustering (Class I) would have a markedly distinct GFP staining pattern around the nuclear rim. In addition, it has also been observed that during the division of mutants with NPC clusters, the clusters are not necessarily divided equally between the resulting mother and daughter cells (Doye *et al.*, 1994; Wente and Blobel, 1994; Heath *et al.*, 1995; Pemberton *et al.*, 1995). This should result in one cell having a substantially lower total fluorescence signal until it forms a new cluster. Mutants that result in fewer total NPCs per nucleus (Class II) would have a reduced total GFP fluorescence signal as compared with wt cells. Such Class II mutants may be in genes encoding global mediators of NPC assembly, as has been proposed for Nic96p (Zabel *et al.*, 1996; Grandi *et al.*, 1997). Finally, mutants that have wt NPC number but with each NPC having a decreased amount of GFP-Nup incorporated (Class III) would also exhibit a decrease in total GFP fluorescence signal.

Because of these potential GFP fluorescence signal differences between wt and the three proposed mutant classes, we predicted that such NPC assembly mutant cells could be physically separated from wt cells using fluorescence-activated cell sorting (FACS). To test the feasibility of FACS selection in mutant isolation, we analyzed by flow cytometry wt, *nup133*Δ, and *nic96–1* mutant cells that expressed GFP-Nup49p. As shown in Figure 1A (red), wt cells not expressing GFP protein have an endogenous low fluorescence emission level (488 nm ex, 530 nm em). In contrast, wt cells expressing GFP-Nup49p have a mean fluorescence emission peak nearly five times greater than the endogenous autofluorescence (Figure 1A, green). Strains bearing a null allele (Δ) of *NUP133* have constitutive NPC clusters at all growth temperatures (Doye *et al.*, 1994; Li *et al.*, 1995; Pemberton *et al.*, 1995). When analyzed by flow cytometry (Figure 1A, blue profile) after growth at 23°C, the *nup133*Δ mutant expressing GFP-Nup49p displayed a strikingly different fluorescence profile from either of the two wt strains. The wt GFP-Nup49p profile was markedly symmetrical with one sharp peak, whereas the *nup133*Δ mutant GFP-Nup49p profile was broader with two distinct peaks. The left-shifted peak was indicative of a fraction of cells with a low GFP signal. The *nup133*Δ cells with low fluorescence may reflect a population of newly divided cells that lack large NPC clusters. The right-shifted peak represented a *nup133*Δ cell population with a greater fluorescence intensity and may therefore reflect cells with large NPC clusters.

Previous studies by Zabel *et al.* (1996) have reported a decreased NPC density in temperature-sensitive *nic96–1* mutant cells. FACS analysis of the temperature-sensitive *nic96–1* mutant expressing GFP-Nup49p also showed perturbations in the flow cytometry pattern compared with wt cells (Figure 1B). When grown at 23°C, the peak for the GFP-Nup49p in *nic96–1* cells (Figure 1B, blue) was shifted to the left and was broader than the profile for wt GFP-Nup49p cells (green). After shifting to growth at 37°C for 5 h, the peak for the *nic96–1* cells remained left-shifted (Figure 1B, orange) compared with wt although it was markedly sharper than the profile for mutant cells at 23°C. Therefore, on the basis of GFP-Nup49p expression, cells harboring known mutant alleles related to NPC assembly have distinct flow cytometric properties as compared with wt cells.

To assess whether the distinct FACS patterns obtained were dependent on using GFP-Nup49p, the

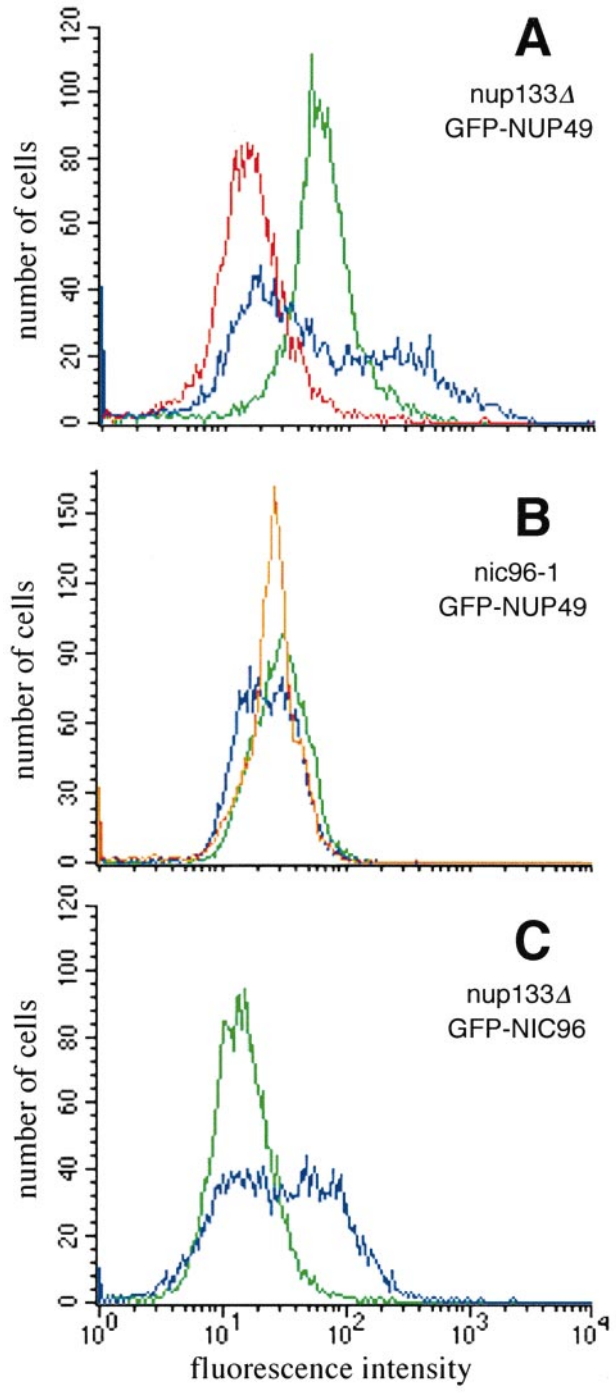

Figure 1. NPC mutants expressing GFP-Nup49p have distinct fluorescence properties compared with wt cells expressing GFP-Nup49p. Flow cytometry analysis was performed on cells grown to logarithmic phase in SD lacking leucine (488 nm ex, 530 nm em). wt strains expressing GFP-Nup49p (SWY894, green profiles in panels A and B) have a fluorescence emission level nearly five times as great as the endogenous fluorescence of cells not expressing GFP (SWY1601, red profile in panel A). (A) *nup133*Δ cells expressing GFP-Nup49p (SWY1667, blue) display a bimodal distribution reflecting two populations of GFP-labeled cells with different fluores-

sequence encoding GFP was fused in frame with the sequence encoding the N terminus of full-length Nic96p. The *GFP-NIC96* gene was integrated in place of the respective chromosomal *NIC96* allele in both wt and *nup133*Δ strains. The FACS peak for wt cells expressing GFP-Nic96p was symmetrical (Figure 1C, green). Interestingly, the profile for GFP-Nic96p *nup133*Δ cells was distinct from wt (Figure 1C, blue) and notably broad as was the case for the GFP-Nup49p *nup133*Δ cells. However, in contrast to the GFP-Nup49p *nup133*Δ profile, the majority of the GFP-Nic96p *nup133*Δ peak was not shifted to the low fluorescence intensity region but rather toward a higher fluorescence level. Therefore, the particular GFP-tagged nucleoporin employed may influence the perturbations observed in a mutant cell's FACS profile. In some cases this may be reflected by functional or physical interactions between the particular nucleoporins. For instance, the established genetic interaction between *nup49* and *nup133* mutant alleles may suggest that there is a physical/functional association between the two nucleoporins (Doye *et al.*, 1994). The FACS results in Figure 1 further suggested that the types of mutants obtained in a FACS-based genetic screen may be dependent on the particular GFP-tagged nucleoporin expressed.

Based on the above rationale and the FACS results, we designed a genetic strategy to identify novel factors required for proper NPC assembly. A flowchart of the strategy is detailed in Figure 2. We focused the strategy on isolating mutants that exhibited a constitutively lowered GFP-Nup49p fluorescence level during growth at 23°C. The choice of GFP-Nup49p was due to our extensive previous analysis of this GFP-tagged nucleoporin (Bucci and Wente, 1997), and the observed FACS shifts to lower fluorescence levels in the known mutant profiles at 23°C (Figure 1). After a primary FACS selection from a chemically mutagenized population of cells, a secondary screen was also included whereby individual colonies resulting from growth at 23°C would be further tested by direct fluorescence microscopy. The microscopic analysis would allow confirmation of a fluorescence perturbation, and the mutants could be coincidentally classed as either NPC clustering mutants (I) or mutants with an overall decrease in GFP-NPC fluorescence intensity (Classes II or III). After identification of mutants, two control experiments were designed to eliminate mutant strains resulting from an indirect loss of GFP

Figure 1 (cont.). cence levels. (B) *nic96–1* cells expressing GFP-Nup49p (SWY1860) show a broad, left-shifted peak after growth at 23°C (blue) and a sharp symmetrical peak after growth for 5 h at 37°C (orange). (C) *nup133*Δ cells expressing GFP-Nic96p (SWY1824, blue) have a distinct profile compared with wt cells expressing GFP-Nic96p (green).

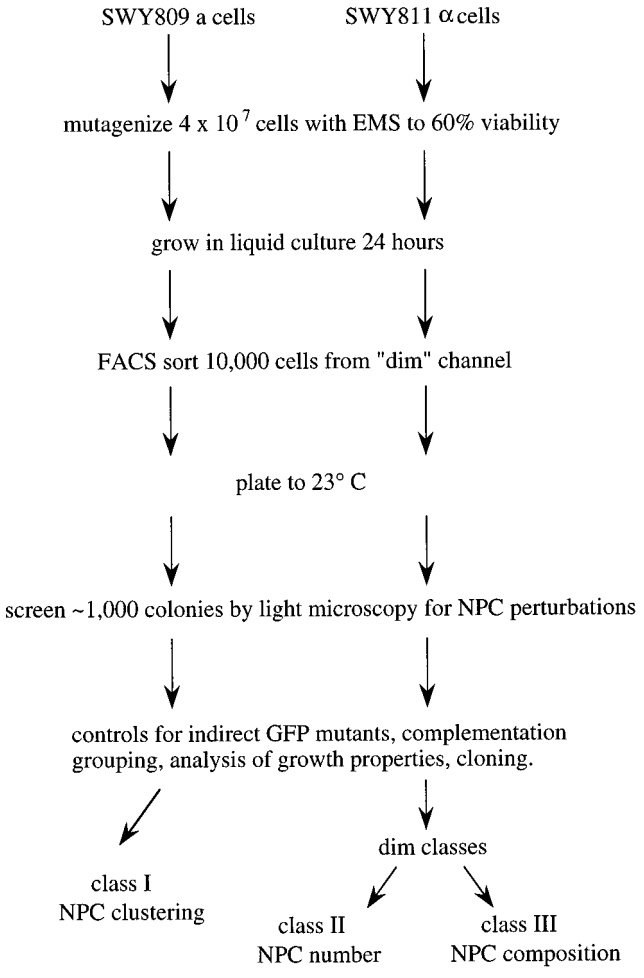

Figure 2. Schematic diagram for a fluorescence-based strategy to isolate NPC assembly mutants. Strains expressing GFP-Nup49p were selected by FACS and screened by microscopic inspection of GFP-NPC fluorescence patterns. Candidate mutants were tested for plasmid-dependent complementation and for growth phenotypes. We predicted that at least three different classes of mutants would be identified: Class I, NPC clustering; Class II, fewer total NPCs per nucleus, and Class III, wt NPC number, but each NPC with a decreased amount of GFP-Nup incorporated.

signal. A lowered fluorescence level (dim) phenotype could be due to mutations within the GFP portion of the GFP-Nup49p fusion itself, and/or nonspecific defects in GFP-Nup49p transcription, translation, or folding. To eliminate mutants due to indirect GFP perturbations, the strains could be tested for complementation of the dim phenotype by 1) transformation and expression of a plasmid-borne copy of *GFP-NUP49* in the haploid mutant, and 2) mating the mutant to a wt strain that does not express GFP-Nup49p. Only dim mutants not rescued by the plasmid transformation but complemented by the mating test would be selected for further analysis. We predicted that such a strategy would result in a focus on the isolation of novel, recessive mutants harboring defects in NPC assembly.

Identification of NPC Assembly Mutants

Following the strategy outlined in Figure 2, a FACS screen to isolate novel mutants with lowered GFP-Nup49p fluorescence was conducted. Isogenic *MAT**a*** and *MATα GFP-NUP49* strains were mutagenized with EMS and allowed to recover in liquid culture before a subpopulation of the cells was subjected to FACS sorting. One percent of the cells with the lowest relative GFP fluorescence were collected and plated for colony growth on rich media at 23°C. Approximately 10% of the estimated 10,000 sorted cells formed colonies, and this correlated well with the results of similar FACS strategies in yeast (Wendland *et al.*, 1996). These strains were each individually screened by fluorescence microscopy for visual perturbations in NPC distribution (clustering phenotypes) or fluorescence intensity levels. Eight mutants were isolated with distinctly perturbed GFP-NPC staining as compared with wt: two (designated C36 and C18) had NPC clusters, and six others exhibited an overall dim (low fluorescence level) phenotype.

Since the strains with a dim phenotype could be due to mutations within GFP itself rather than defects in NPC assembly, a plasmid-borne copy of *GFP-NUP49* (pSW636) was transformed into the six dim strains. The dim phenotype in strains defective for NPC assembly should not be complemented by this plasmid. Five of the dim strains were rescued to nearly wt GFP-NPC staining with plasmid-borne GFP-Nup49p (our unpublished observations) and were likely due to a direct mutation in GFP. These strains were not further analyzed. The remaining dim mutant (E17) was not complemented by plasmid-expressed GFP-Nup49p and was possibly due to a direct defect in NPC assembly. Fluorescence microscopy analysis of wt cells and the E17 and C36 mutants is shown in Figure 3. The fields were exposed and printed for identical times to accurately reflect the intensity and distribution differences in the GFP-Nup49p signal. The signal for the wt parental cells (upper panel) is localized over the entire nuclear rim in a punctate pattern typical for nucleoporin localization. The middle panels show the clustering phenotype of the *nup133*Δ and the C36 mutant, where the majority of the GFP-Nup49p signal is concentrated in discrete foci representing brightly labeled NPC clusters. The dim phenotype of the E17 mutant strain (Figure 3, lower panel) reflects an overall lower GFP intensity in the NE. The dim phenotype is completely penetrant, with all cells in the population showing similarly low GFP intensities.

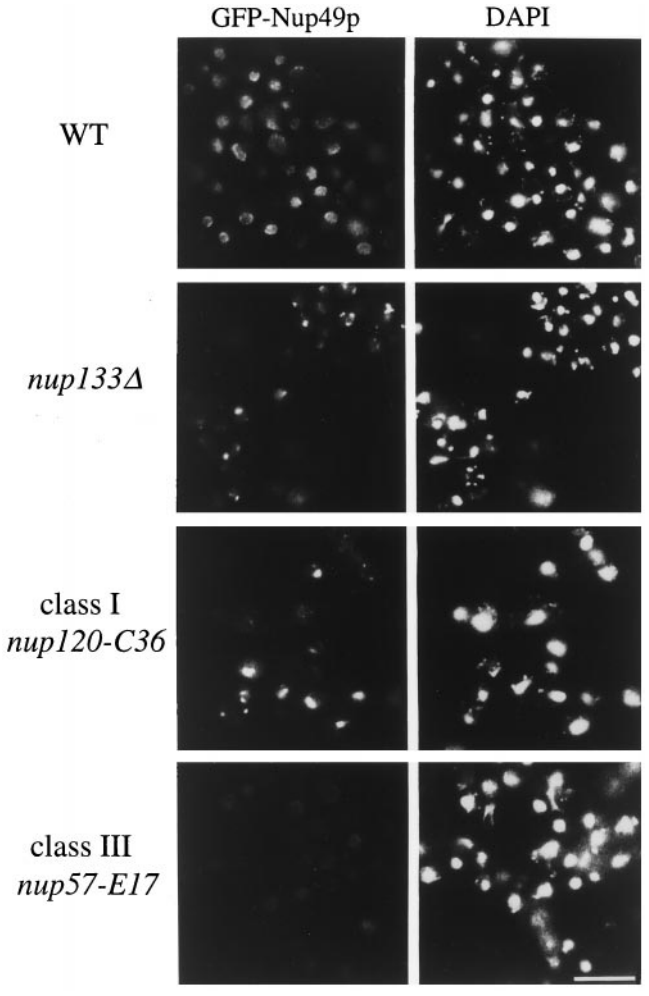

Figure 3. Two classes of NPC mutants were isolated in the GFP-Nup49p fluorescence-based strategy: NPC clustering mutants and dim mutants. Direct fluorescence microscopy analysis of GFP-Nup49p localization in wt, *nup133*Δ, and two representative mutant strains isolated in the FACS-based screen. The strains were grown in SD media lacking leucine: wt (SWY894), *nup133*Δ clustering (SWY1667), clustering-Class I (*nup120-C36* mutant, SWY1710), Dim-Class III (*nup57-E17* mutant, SWY1708). Within each column, photographs were exposed and printed for identical times. DAPI staining for each respective field is shown on the left. Bar, 10 μm.

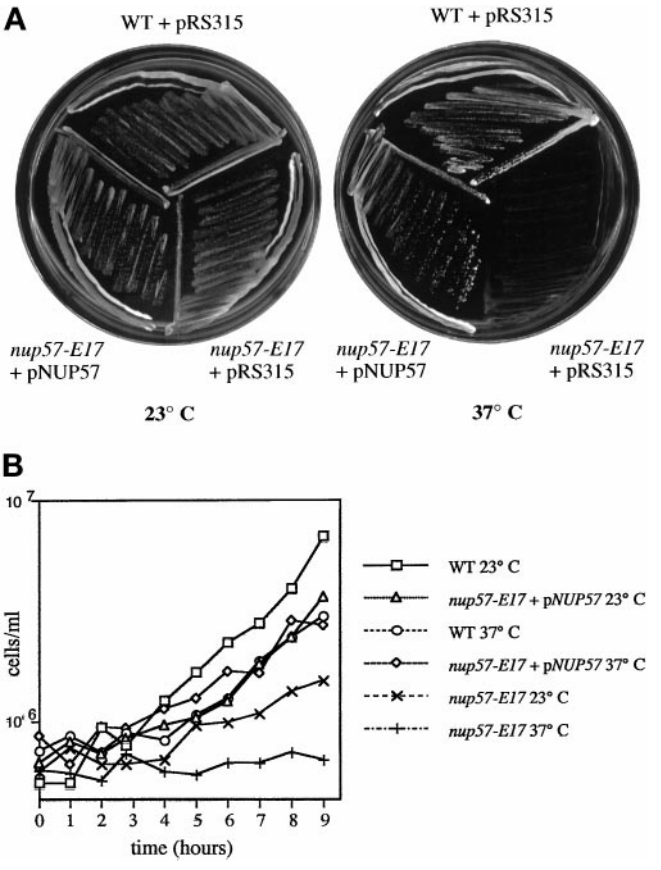

Figure 4. Expression of *NUP57* from a plasmid complements the temperature sensitivity of the *nup57-E17* mutant. (A) Strains were grown on SD plates lacking leucine for 4 d at 23 or 37°C: wt (SWY894), *nup57-E17* with pRS315 (SWY1708), *nup57-E17* + pSW806/*NUP57* (SWY1709). *NUP57* expression restores growth to the *nup57-E17* strain at 37°C. (B) Growth analysis of wt, *nup57-E17*, and *nup57-E17* + *NUP57* cells at 23 and 37°C. Aliquots of cells growing at early logarithmic phase were counted at various time points after shift to 37°C or continued growth at 23°C. Cell counts are expressed as cell number per ml of culture.

Complementation Analysis Reveals Mutant Alleles of nup120, gle2, and nup57

The E17 dim mutant and the C36 and C18 clustering mutants were chosen for further characterization. All three represented alleles in distinct complementation groups, as determined by analyzing the phenotype of diploids formed from pairwise crosses of the respective mutants in *MAT***a** or *MAT*α backgrounds. In addition, the C36, C18, and E17 mutants were all temperature-sensitive for growth at 37°C (Figure 4, and our unpublished observations). The temperature sensitivity was also genetically linked with the GFP phenotypes (as determined by backcrossing to the wt parental strains).

To test whether the C36, C18, and E17 mutants were due to mutations in genes encoding known NPC-associated factors, the strains were each transformed with a bank of *CEN/LEU2* plasmids harboring known genes and tested for complementation of the mutant phenotype. Both the temperature sensitivity and the clustering phenotypes of the C36 mutant were complemented by a wt *NUP120* gene. Moreover, the temperature sensitivity and the NPC clustering of C36 cells were not complemented after mating to a strain harboring a null allele of *NUP120* (CHY104). Similarly, the C18 mutant also represented a mutation in a gene encoding a known NPC-associated factor. The temperature sensitivity and clustering phenotypes of the C18 mutant were complemented by a plasmid harboring

GLE2. In addition, the C18 phenotypes were not complemented by mating to a *gle2*Δ strain (SWY1226). Since the *NUP120* and *GLE2* plasmids complemented the GFP phenotypes of the C36 and C18 mutants, respectively, we compared mutant strains with or without a complementing plasmid to wt strains in flow cytometry experiments. Figure 5, A and B, shows the fluorescence histograms for these two mutants transformed with either the complementing gene (red) or an empty vector (blue). The *nup120-C36* mutant histogram (Figure 5A) is remarkably symmetrical compared with that for the *nup133*Δ strain shown in Figure 1A; one major peak corresponding to an overall decrease in GFP intensity was observed (blue). When the *NUP120* plasmid was expressed in the *nup120-C36* cells, the FACS peak was shifted to the right overlapping the wt peak and reflected greater GFP intensity (Figure 5A, red). The *gle2-C18* mutant profile was very similar of that observed with *nup133*Δ cells as reflected by the two broad peaks (Figure 5B, blue). When the *gle2-C18* strain harbored the *GLE2* plasmid, the profile shifted to a single peak with a fluorescence intensity comparable to wt (Figure 5B, red). Mutant alleles of *nup120* (Aitchison *et al.*, 1995; Heath *et al.*, 1995) and *gle2* (Murphy *et al.*, 1996) that result in NPC clusters have been previously reported. The differences we observed between the GFP-Nup49p FACS profiles in different clustering mutants may reflect true distinctions between the clustering types. Indeed, the fluorescence microscopy analysis of the mutants (Figure 3) shows the majority of the *nup120-C36* cells with clusters have a single large foci of GFP-NPC staining, whereas the clusters in *nup133*Δ cells are smaller and are often numerous. Alternatively, the distinct profile may also be related to the expression of GFP-Nup49p and perturbations of possible interactions with the given mutant nucleoporin Nup133p, Nup120p, or Gle2p.

Interestingly, the temperature-sensitive E17 dim mutant was complemented by a plasmid harboring *NUP57* (Figures 4A and 5C). Figure 5, C and D, shows the analysis of two dim mutants: a mutant (D66) representing the group due to mutations in GFP (Figure 5D, orange) and the *nup57-E17* dim mutant (Figure 5C, blue). For both, a single broad peak of lowered fluorescence intensity was observed compared with wt cells (green profiles). When the plasmid encoding *NUP57* was expressed in the *nup57-E17* mutant and cells grown at 23°C were analyzed, the main peak shifted from a low fluorescence intensity (Figure 5C, blue) (comparable to cells expressing no GFP protein) to a higher fluorescence intensity (Figure 5C, red). However, the profile for the *nup57-E17* cells expressing *NUP57* did not match the wt profile (green). In addition, when the cells were analyzed for relative growth rates, full complementation was not observed at 23°C (Figure 4B). These results suggested that at 23°C the mutant nup57p^{E17} protein was competing with the wt Nup57p for incorporation into the NPC. Interestingly, when the *nup57-E17* cells harboring the *NUP57* plasmid were shifted to growth at 37°C, full complementation was observed as reflected by the overlapping growth curves for both wt and *nup57-E17* + *NUP57* cells at 37°C (Figure 4B). Moreover, the FACS profile at 37°C for *nup57-E17* + *NUP57* cells (Figure 5C, orange) was also coincident with that for wt (green). Overall, the isolation of known clustering and nucleoporin mutants validates our approach of mutagenizing a wt culture and using a FACS and fluorescence screening strategy to identify genes related to NPC structure.

NPC Incorporation of GFP-Nup49p Is Inhibited in the nup57-E17 Mutant

We predicted that further analysis of the *nup57-E17* mutant would provide a unique opportunity to analyze the role of Nup57p in vivo. Nup57p belongs to the GLFG family of nucleoporins (Wente *et al.*, 1992; Grandi *et al.*, 1995b), in which each member is characterized by amino-terminal regions with multiple GLFG tetrapeptide repeats separated by uncharged spacer sequences. Studies by others have documented that Nup57p forms a heterotrimeric complex with Nup49p and Nsp1p both in vitro and in immunoprecipitates from yeast cell lysates (Grandi *et al.*, 1995b; Schlaich *et al.*, 1997). Since Nup49p and Nup57p directly interact in vitro (Schlaich *et al.*, 1997), the *nup57-E17* phenotype was possibly due to fewer GFP-Nup49p molecules incorporated per NPC instead of a decrease in total NPC number per nucleus. If total NPC number had been substantially changed, we predicted that NPC staining for Pom152p would be coincidentally decreased. Pom152p is an integral membrane protein localized to the pore membrane (Wozniak *et al.*, 1994). Indirect immunofluorescence microscopy was performed with a monoclonal antibody (mAb) recognizing Pom152p (Strambio *et al.*, 1995). The staining level and pattern of anti-Pom152p was identical in wt and *nup57-E17* cells grown at either 23 or 37°C (Figure 6, bottom panel). In comparison, when GFP-Nup49p was expressed in wt and *nup57-E17* mutant strains, the NPC-associated GFP-Nup49p was greatly diminished in mutant cells as compared with wt (Figure 6, top panel). This suggested that the lack of GFP-Nup49p incorporation in the *nup57-E17* mutant did not reflect a total inhibition of NPC and nuclear pore assembly. Thus, the *nup57-E17* allele likely represented a Class III mutant with approximately wt NPC number but with each NPC having a decreased level of GFP-Nup49p incorporated.

To test whether the diminished GFP-Nup49p level in *nup57-E17* cells was due to degradation of GFP-

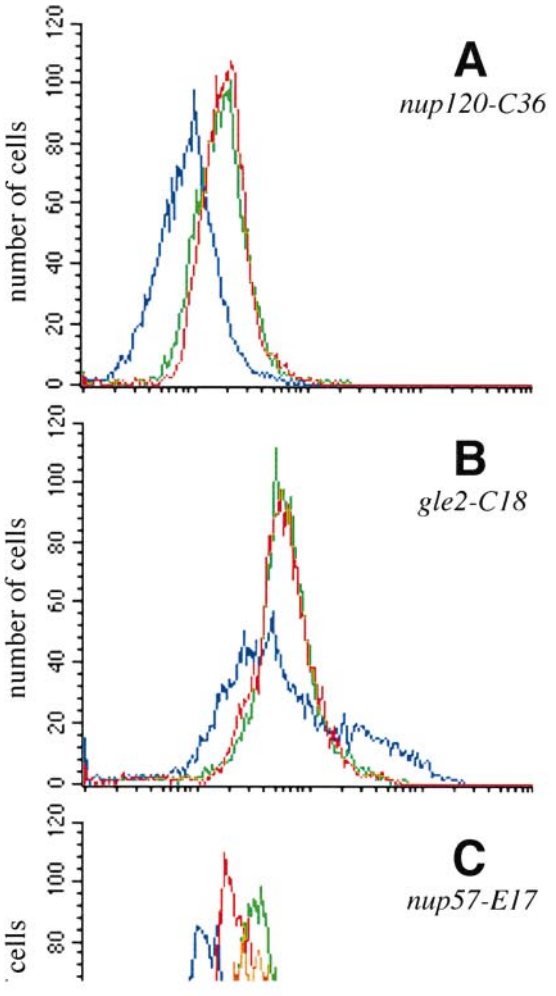

Nup49p, whole yeast cell lysates from wt and mutant cells were immunoblotted with an anti-GFP antibody (Figure 7A, lower panel). When the cells were grown at the permissive temperature, the GFP-Nup49p levels were similar in wt and *nup57-E17* strains (lanes 1 and 8, respectively). Considering the lowered total fluorescence level measured by FACS, the high levels of GFP-Nup49p in *nup57-E17* cells seemed paradoxical. The level of GFP-Nup49p fluorescence signal was not sensitive to fixation with formaldehyde as similar results were obtained by FACS and microscopy regardless of whether or not the *nup57-E17* cells were fixed (our unpublished observations). This suggested that at 23°C unincorporated GFP-Nup49p was stable and that the lack of assembly and concentration at the NPC (and presumed cytoplasmic localization, see below and Figure 8) did not contribute to the total FACS-analyzed GFP fluorescence levels of *nup57-E17* cells. GFP-Nup49p that is not properly assembled into the NPC may not fold correctly for detectable fluorescence by either FACS or direct fluorescence microscopy.

Identical cell lysate samples from the wt and *nup57-E17* cells were also probed with an affinity-purified polyclonal antibody raised against the GLFG region of Nup116p that preferentially detects both Nup116p and Nup57p. In general, the relative levels of Nup116p and Nup57p or nup57p^{E17} appeared similar between wt and mutant cells at 23°C (Figure 7A, upper panel). Interestingly, the nup57p^{E17} protein migrated faster than the wt Nup57p. Since the *nup57-E17* mutant was lethal at 37°C, cell lysates were also analyzed after growth at the nonpermissive temperature for various times (Figure 7A, compare lanes 9–14 with lanes 2–7). At the early time points of 15, 30, or 60 min, nup57p^{E17} was present. However, after 2 h at 37°C, the nup57p^{E17} signal was virtually undetectable. Levels of GFP-Nup49p decreased in a similar manner coincident with the loss of nup57p^{E17} at 37°C. To address the reversibility of the temperature-induced growth defect, after growth at 37°C the *nup57-E17* cells were plated and grown at 23°C (Table 2). Viability of the mutant decreased substantially between the 2- and 3-h time points, indicating the growth defect was irreversible once GFP-Nup49p and nup57p^{E17} were degraded. These results further support a model wherein at 23°C